Volume 12
Number 8
21 April 2025
Pages 2401–2748

Materials Horizons

rsc.li/materials-horizons

ISSN 2051-6347

ROYAL SOCIETY OF CHEMISTRY

COMMUNICATION

Rodrigo E. Palacios, Miryam Criado-Gonzalez *et al.*
Poly(3-hexylthiophene) nanoparticles as visible-light photoinitiators and photosensitizers in 3D printable acrylic hydrogels for photodynamic therapies

Materials Horizons

ROYAL SOCIETY OF CHEMISTRY

COMMUNICATION

View Article Online
View Journal | View Issue

Cite this: *Mater. Horiz.*, 2025, **12**, 2524

Received 10th December 2024,
Accepted 3rd March 2025

DOI: 10.1039/d4mh01802h

rsc.li/materials-horizons

Poly(3-hexylthiophene) nanoparticles as visible-light photoinitiators and photosensitizers in 3D printable acrylic hydrogels for photodynamic therapies†

Rocío Natera Abalos,[a] Ilaria Abdel Aziz,[b] Matías Caverzan,[a] Arianna Sosa Lochedino,[a] Luis E. Ibarra,[c] Antonela Gallastegui,[b] Carlos A. Chesta,[a] M. Lorena Gómez,[a] David Mecerreyes,[bd] Rodrigo E. Palacios *[a] and Miryam Criado-Gonzalez *[be]

The design of smart photoelectrodes capable of stimulating the localized production of reactive oxygen species (ROS) on demand is of great interest for redox medicine therapies. In this work, poly(3-hexylthiophene) semiconducting polymer nanoparticles (P3HT SPNs) are used with a dual role to fabricate light-responsive hydrogels. First, P3HT SPNs act as visible-light photoinitiators to induce the photopolymerization of acrylic monomers such as acrylamide (AAm), 2-(hydroxyethyl) acrylate (HEA), and poly(ethylene glycol) diacrylate (PEGDA). This leads to the formation of acrylic hydrogels loaded with the P3HT SPNs, as demonstrated by photo-rheology and infrared spectroscopy. Furthermore, P3HT SPNs are also successfully used as photoinitiators for digital light processing (DLP) 3D printing purposes to fabricate shape-defined intelligent hydrogels. Interestingly, P3HT SPNs retain their photoelectrochemical properties when embedded within the polymer hydrogels, showing photocurrent densities that range from ~0.2 to ~1.1 μA cm^{-2} depending on the intensity of the visible light-lamp (λ = 467 nm). Second, they can be used as photosensitizers (PS) to generate reactive oxygen species (ROS), 12–15 μM H_2O_2, on demand. The acrylic hydrogels containing P3HT SPNs do not exhibit cytotoxic effects under normal physiological conditions in the darkness against mouse glioma 261 (GL261) cells and *S. aureus* bacteria. However, they induce a ~50% reduction GL261 cancer cell viability and a ~99% *S. aureus* cell death in contact with them upon illumination (λ = 467 nm) due to the localized overproduction of ROS, which makes them attractive candidates for photodynamic therapies (PDT).

New concepts

In this work, we demonstrate the concept of smart light-responsive hydrogels for photodynamic therapies (PDT) through the employment of poly(3-hexylthiophene) semiconducting polymer nanoparticles (P3HT SPNs). The excellent optoelectronic properties of P3HT SPNs are exploited with a dual role to act as (i) efficient and highly biocompatible visible light photoinitiators (PIS) for the polymerization of acrylic hydrogels and (ii) photosensitizers (PS) to trigger the overproduction of ROS (12–15 μM H_2O_2). Unlike traditional PIS, P3HT SPNs do not precise toxic co-initiators, while they retain their photocurrent properties when embedded within the acrylic hydrogels for proven PDT and future *in situ* bioprinting purposes. Furthermore, P3HT SPNs are used as PIS ($\lambda > 405$ nm) during the digital light processing (DLP) 3D printing of high-resolution hydrogels towards personalized scaffolds for post-surgical tissue defects reparation. The P3HT SPNs containing hydrogels succesfully reduce a ~50% mouse glioma (GL261) cancer cell viability and a ~99% *S. aureus* bacteria viability in a spatial-temporal controlled manner upon visible light illumination ($\lambda > 467$ nm) due to the localized overproduction of ROS. In conclusion, the intelligent P3HT acrylic hydrogels are a new class of promising materials for PDT against both cancer and bacteria, offering unique advantages over traditional materials reported in the literature.

1. Introduction

Reactive oxygen species (ROS) are biologically relevant oxidants for redox medicine. While a moderate increase in the ROS levels can regulate the fates of endothelial cells promoting tissue regeneration, excessive ROS production (*i.e.*, hydrogen peroxide (H_2O_2)) triggers oxidative stress resulting in cell

[a] *Instituto de Investigaciones en Tecnologías Energéticas y Materiales Avanzados (IITEMA), Universidad Nacional de Río Cuarto (UNRC) and Consejo Nacional de Investigaciones Científicas y Tecnológicas (CONICET), Campus Universitario, 5800 Río Cuarto, Argentina. E-mail: rpalacios@exa.unrc.edu.ar*
[b] *POLYMAT, University of the Basque Country UPV/EHU, Joxe Mari Korta Center. Avda. Tolosa 72, 20018, Donostia-San Sebastián, Spain. E-mail: miryam.criado@ehu.eus*
[c] *Instituto de Biotecnología Ambiental y Salud (INBIAS), Universidad Nacional de Río Cuarto (UNRC) and Consejo Nacional de Investigaciones Científicas y Tecnológicas (CONICET), Campus Universitario, 5800 Río Cuarto, Argentina*
[d] *Ikerbasque, Basque Foundation for Science, 48013 Bilbao, Spain*
[e] *Institute of Polymer Science and Technology (ICTP-CSIC), 28006 Madrid, Spain*

† Electronic supplementary information (ESI) available: ^{1}H NMR spectrum of P3HT; TEM image and UV-vis spectrum of P3HT SPNs; rheological properties of hydrogels; fluorescence pictures of hydrogels; fluorescence microscopy images GL261 cell viability and ROS production tests; flow cytometry results. See DOI: https://doi.org/10.1039/d4mh01802h

dysfunction and apoptosis.[1–3] This is of paramount importance in the case of cancer cells that produce higher levels of ROS than normal cells. This elevated ROS can be targeted by anticancer therapies that stimulate additional ROS production, pushing cancer cells to their limit and eventually killing them.[4,5] This is the mechanism behind photodynamic therapy (PDT), a minimally invasive clinical treatment that combines photosensitizers (PS) in conjunction with appropriate light wavelengths and molecular oxygen to generate enough ROS to induce cell apoptosis.[6] Mainly due to superb spatial-temporal control of light, PDT enables enhanced tumor therapeutic efficacy and targeting compared to conventional cancer therapies, minimizing side effects in healthy tissues. Moreover, PDT can also be applied after surgical resection to eliminate remaining cancer cells at the site, which is key for glioblastomas (GBM), one of the most aggressive tumors of the central nervous system with resistance to conventional radio- and chemotherapies.[7,8] Another interesting aspect to be considered is the possibility of replacing and regenerating the post-surgical tissue defects for faster patient recovery.[9,10] This can be achieved with the employment of printable hydrogel-based scaffolds that can mimic the shape and mechanical properties of the damaged tissues while providing ideal conditions for nutrient transportation and cell ingrowth ensuring a faster regeneration.[11–13] In recent years, 3D printing technologies have emerged as powerful manufacturing methods to fabricate low-cost, customizable, and complex 3D biomedical scaffolds with micrometric precision.[14,15] When stimuli-responsive materials are employed the process is referred to as 4D-printing.[16,17] Among them, digital light processing (DLP) 4D printing is attracting increasing attention due to the high resolution of the intelligent printed scaffolds. For such a purpose, light-induced printable inks require a resin containing acrylic monomers and photoinitiator systems (PIS) able to generate free radicals to initiate a fast photopolymerization upon light activation.[18,19] While water-soluble type I and type II PIS are the most commonly used PIS for biomedical applications, they present some limitations. Type I PIS require UV light for activation and type II PIS a co-initiator, which usually is toxic (*e.g.*, amines, onium salts), that donates electrons or hydrogen, hampering their use in clinical trials.[20,21] Very recently, we reported the employment of conjugated polymer (CP) nanoparticles as visible-light panchromatic PIS of acrylic monomers in water.[22–24] Among different types of CPs, poly(3-hexylthiophene) (P3HT) is the gold standard of p-type semiconducting polymers for (bio-opto)electronic applications. It is commercially available at a competitive price and possesses excellent optoelectronic properties to act as an efficient and highly biocompatible phototransducer when processed both in the form of thin films and as nanoparticles.[25–28] Nevertheless, to the best of our knowledge, the development of 3D printable hydrogels containing P3HT has not been reported nor has their application for PDT against cancer. These features make P3HT semiconducting polymer nanoparticles (SPNs) valuable players to be explored as both photoinitiator systems (PIS) and photosensitizers (PS) for redox active hydrogels. In this work we show that P3HT SPNs can act as (i) visible light PIS for the photopolymerization and 3D printing of stimuli-responsive acrylic polymer hydrogels relevant for biomedicine, and (ii) active PS to trigger the overproduction of ROS from hydrogels for PDT against GBM cells and *S. aureus* bacteria (Scheme 1).

2. Results and discussion

The ability of P3HT SPNs to generate radicals was harnessed for use as photoinitiator systems (PIS) for the polymerization of acrylic monomers (AAm, HEA, and PEGDA) in aqueous media leading to the formation of hydrogels (Scheme 1). The employment of P3HT SPNs as PIS does not require co-initiators, while they also act as cross-linkers when excited in the visible and near UV range (Fig. S2B, ESI†). To explore this, first, the effect of the P3HT SPNs concentration (x = 5, 80 and 105 mg mL^{-1}) on the formation of acrylic polymer hydrogels, PEGDA-SPNs$_x$, was studied by photorheology (Fig. 1A). This technique allowed us to determine the gelation point ($G' = G''$), where the crossover between the liquid-like state ($G'' > G'$) and the solid-like state ($G' > G''$) takes place, thus pointing out the formation of the PEGDA-SPNs$_x$ hydrogels. At the lowest SPNs concentration (5 mg mL^{-1}), the gelation process of PEGDA-SPNs$_5$ was very slow ($\sim$80 min). As the concentration of SPNs increased, the gelation occurred faster. At the intermediate SPNs concentration (80 mg mL^{-1}), the formation of PEGDA-SPNs$_{80}$ hydrogels occurred in $\sim$45 min due to both the higher number of radicals produced during the irradiation process and the higher number of crosslinks. At the highest SPNs concentration (105 mg mL^{-1}), the gelation process of PEGDA-SPNs$_{105}$ hydrogels was also favored but slower ($\sim$65 min) than in the previous case. This can be attributed to different factors such as radical-radical annihilation due to a higher number of radicals produced, and/or

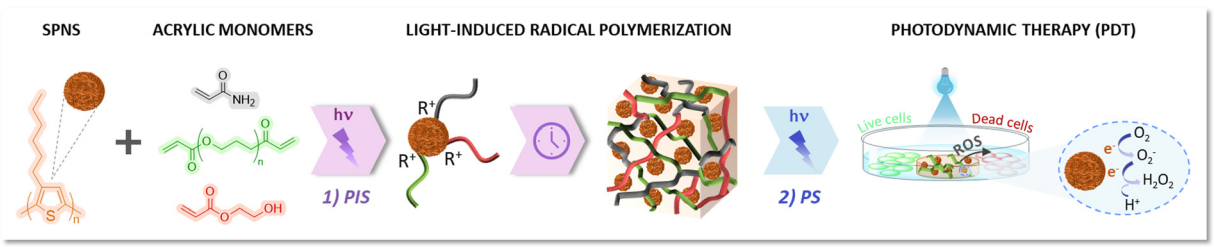

Scheme 1 Dual role of P3HT SPNs as (1) photoinitiators (PIS) of the light-induced radical polymerization of acrylic monomers for the synthesis of photo-responsive hydrogels, and (2) photosensitizers (PS) to generate reactive oxygen species (ROS) on demand for photodynamic therapies (PDT).

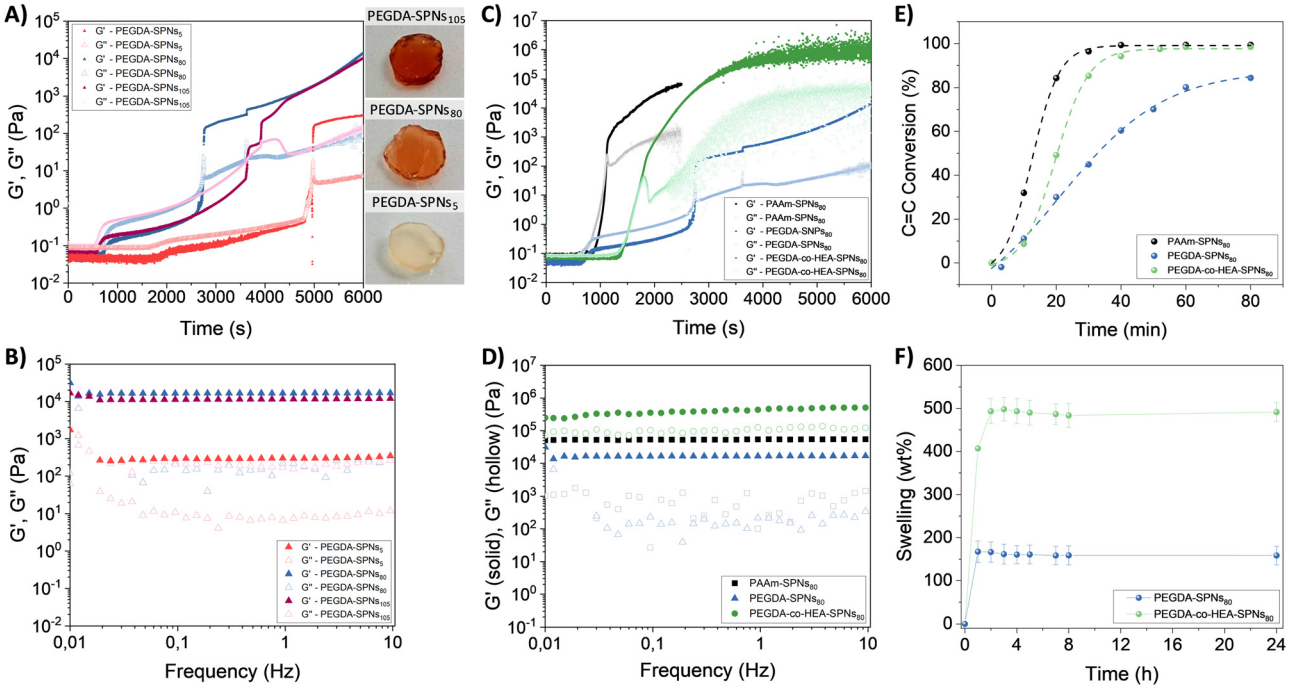

Fig. 1 (A) Evolution of G' and G'' of PEGSA-SPNs$_x$ as a function of irradiation time (λ = 365 nm, 20 mW cm^{-2}) for different concentrations of SPNs$_x$ (x = 5, 80 and 105) (left). Pictures of the synthesized hydrogels with different SPNs concentrations (right). (B) Elastic (G') and Loss (G'') moduli of PEGDA-SPNs$_x$ hydrogels as a function of the frequency. (C) Evolution of G' and G'' of PEGSA-SPNs$_{80}$, PAAm-SPNs$_{80}$, and PEGSA-*co*-HEA-SPNs$_{80}$ as a function of irradiation time (λ = 365 nm, 20 mW cm^{-2}). (D) Elastic (G') and Loss (G'') moduli of PEGSA-SPNs$_{80}$, PAAm-SPNs$_{80}$, and PEGSA-*co*-HEA-SPNs$_{80}$ hydrogels as a function of the frequency. (E) Conversion of the C=C vinyl double bond of a monomer (AAm), a polymer (PEGDA) and a prepolymer mixture (PEGDA + HEA) as a function of irradiation time (λ = 390 nm, 10 mW cm^{-2}), using SPNs as photoinitiators. (F) Swelling (wt%) of PEGDA-SPNs$_{80}$ and PEGDA-*co*-HEA-SPNs$_{80}$ hydrogels in PBS (pH 7.4) over time.

the prevention of the growth of long polymer chains to form a gel due to the presence of a higher number of SPNs in the media. In all cases, hydrogels with good consistency, colored in red and translucent were formed. The mechanical properties of the synthesized hydrogels were further characterized by oscillatory rheology (Fig. 1B). The elastic modulus (G') of the synthesized hydrogels increased with the SPNs concentration, from 3 × 10^2 Pa for PEGDA-SPNs$_5$ to 1 × 10^4 Pa for PEGDA-SPNs$_{105}$ and remained stable over the whole frequency range. Besides, PEGDA-SPNs$_5$ hydrogels remained stable ($G' > G''$) up to 200% strain, whereas the linear viscoelastic regime decreased for PEGDA-SPNs$_{80}$ and PEGDA-SPNs$_{105}$ hydrogels up to 70% strain due to their higher crosslinking degree and lower flexibility (Fig. S3A, ESI†).

The effectiveness of P3HT SPNs as PIS of other acrylic monomers was also investigated by photo-rheology (Fig. 1C and Fig. S3B, ESI†). In the case of the acrylamide monomer (AAm), the formation of PAAm-SPNs$_{80}$ hydrogels was much faster (~20 min) than in the case of the PEGDA-SPNs$_{80}$ hydrogels (~45 min). This can be explained by the fact that in the case of PEGDA (M_n 525 g mol^{-1}) the chains to be crosslinked by radical polymerization were longer than in the case of AAm (M_W = 71.1 g mol^{-1}) which restricted the formation of crosslinking points slowing down the gelation process. In the third case, the gelation of a mixture comprising a diacrylate polymer (PEGDA) and an acrylic monomer (HEA) was studied. The formation of PEGDA-*co*-HEA-SPNs$_{80}$ hydrogels was faster (~27 min) than PEGDA-SPNs$_{80}$ hydrogels but slower than PAAm-SPNs$_{80}$ hydrogels, as expected due to the combination of both the presence of initial longer chains of PEGDA (M_n 525 g mol^{-1}), but in lower quantity (25%v/v) than in the case of PEGDA-SPNs$_{80}$ hydrogels (50%v/v) as they are mixed with a monomer (HEA) of lower M_w (116.1 g mol^{-1}), leading to an intermediate production of intramolecular and intermolecular crosslinking points. The mechanical properties of the hydrogels were further studied by oscillatory rheology (Fig. 1D). Both PEGDA-SPNs$_{80}$ and PEGDA-*co*-HEA-SPNs$_{80}$ hydrogels ($G' > G''$) were stable over the whole frequency range. PEGDA-*co*-HEA-SPNs$_{80}$ hydrogels exhibited a higher elastic modulus ($G' \sim 3 \times 10^5$ Pa) than PEGDA-SPNs$_{80}$ hydrogels ($G' \sim 1 \times 10^4$) Pa due to their lower crosslinking degree. The effect of SPNs increased concentration in the mechanical properties of PEGDA-*co*-HEA-SPNs$_{105}$ hydrogels was also investigated (Fig. S4, ESI†). Both PEGDA-*co*-HEA-SPNs$_{80}$ and PEGDA-*co*-HEA-SPNs$_{105}$ hydrogels exhibited good flexibility when manipulated with a tweezer (see Fig. S4A, ESI†). However, G' experienced a decrease from ~3 × 10^5 Pa for PEGDA-*co*-HEA-SPNs$_{80}$ to ~3 × 10^4 Pa for PEGDA-*co*-HEA-SPNs$_{105}$ hydrogels (Fig. S4B, ESI†). In agreement with the crosslinking dynamics, we attribute this result to self-deactivation of radicals and/or to the formation of less crosslinked hydrogels, due to a higher number of SPNs that hinders the growth of long polymer chains. These less crosslinked hydrogels broke earlier during

increasing oscillation strains, as corroborated by the lower yield strain (γ'_0, point at which $G' = G''$) values of PEGDA-*co*-HEA-SPNs$_{105}$ ($\gamma'_0 \sim 14\%$) than PEGDA-*co*-HEA-SPNs$_{80}$ ($\gamma'_0 \sim 6\%$) hydrogels (Fig. S4C, ESI†).

To confirm the ability of P3HT SPNs to photoinduce the polymerization of those acrylic monomers and/or polymers in aqueous solution, polymerization kinetics were followed by FT-IR, monitoring the consumption of the vinyl C=C band located at ~6180 cm^{-1} (Fig. 1E). In all cases, the prepolymer mixture contained a concentration of SPNs of 80 mg mL^{-1} and were irradiated with a blue LED (390 nm, 10 mW cm^{-2}). In agreement with photo-rheology results, PAAm-SPNs$_{80}$ showed the fastest polymerization kinetic reaching a 100% conversion in ~30 min, just followed by PEGDA-*co*-HEA-SPNs$_{80}$ that achieved a full conversion after 40 min of irradiation. Finally, PEGDA-SPNs$_{80}$ exhibited the slowest polymerization kinetic reaching a 80% conversion in 80 minutes. This is characteristic of polymeric materials synthesised with diacrylate monomers such as PEGDA, which can also act as a crosslinker, and affect the conversion due to differences in mobility and accessibility to C=C double bonds by the polymeric chains in formation. Thus, it could be confirmed that SPNs have the capacity to act as PIS, photoiniciating the radical polymerization of AAm, PEGDA and HEA monomers in aqueous media, with high monomer conversion yields (80–100%), which led to the formation of hydrogels.

The swelling properties of the hydrogels were further characterized by weight changes when immersed in PBS (pH 7.4) over time (Fig. 1F). The swelling of both PEGDA-SPNs$_{80}$ and PEGDA-*co*-HEA-SPNs$_{80}$ hydrogels occurred immediately in less than 1 minute. However, the swelling degree was higher for PEGDA-*co*-HEA-SPNs$_{80}$ (~600 wt%) than for PEGDA-SPNs$_{80}$ (~170 wt%) hydrogels. This can be attributed to the more polar nature of HEA, with hydroxyl end groups, than PEGDA, thus allowing PEGDA-*co*-HEA-SPNs$_{80}$ hydrogels to hold more water. This behavior has also been observed for other hydrogel systems obtained by copolymerization of HEA with a difunctional monomer from ethylene glycol and thioetheracrylate (EG$_n$SA) using a commercial photinitiator (Darocur).[29]

The design of materials with the ability to be processed into 3D scaffolds with complex structures is actively searched in the biomedical field for personalized medicine purposes.[30] In this regard, the ability of P3HT SPNs to be used as PIS for digital light printing (DLP) processes was also assessed (Fig. 2A). First, the optimal printing conditions were investigated (100 μm layer height and 120 s irradiation per layer) to obtain high-resolution 3D printed scaffolds with shape-defined morphologies and the characteristic red colour of P3HT SPNs (Fig. 2B). The optical properties of the hydrogels were characterized by UV-vis spectrophotometry (Fig. 2C). Both PEGDA-SPNs$_{80}$ and PEGDA-*co*-HEA-SPNs$_{80}$ hydrogels showed similar absorption spectra with a maximum located at 460 nm and a shoulder at 605 nm, which are typical of P3HT SPNs.[28] These results demonstrate that P3HT SPNs embedded in the final hydrogels retain their optical properties after being irradiated to act as PIS. It was also observed that the optical absorption intensity increased with the concentration of SPNs within the hydrogels (Fig. S5, ESI†).

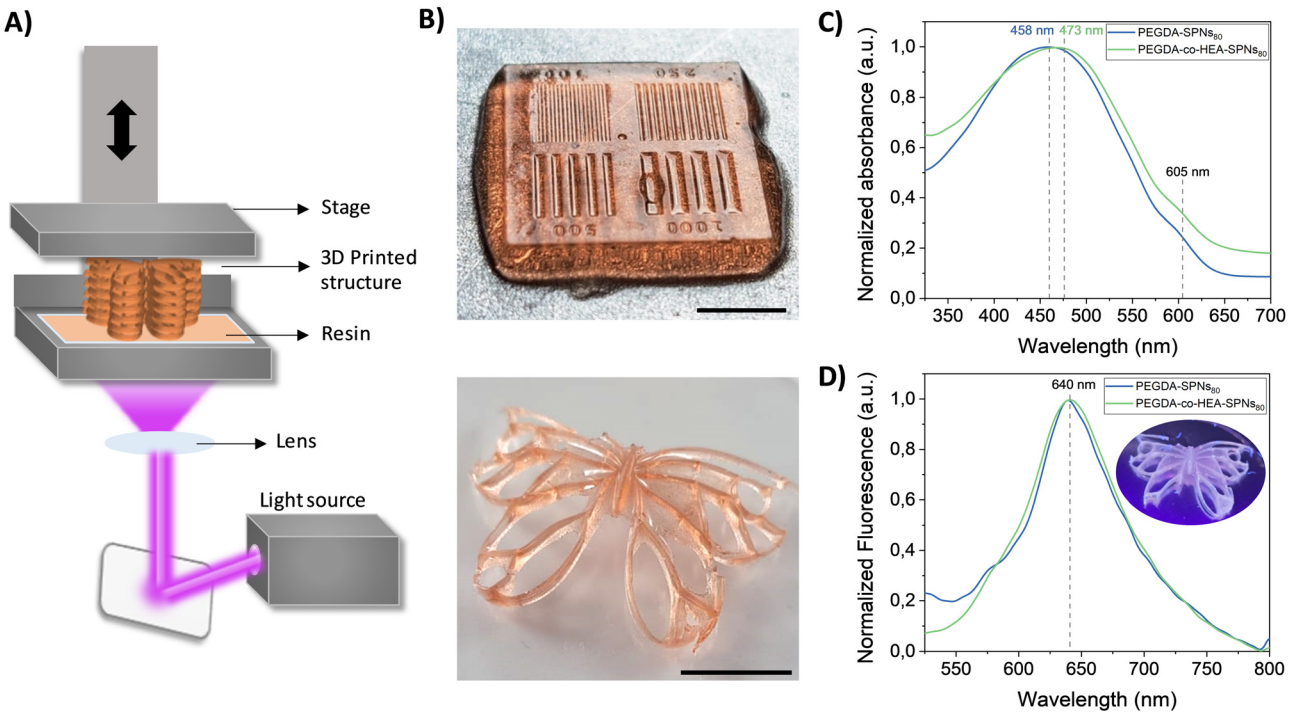

Fig. 2 (A) Schematic representation of the DLP 3D printing process of the prepolymer resin. (B) Pictures of different shape-defined 3D printed hydrogel structures. Scale bars = 5 mm (C) UV-vis spectra and (D) Fluorescence spectra of PEGDA-SPNS$_{80}$ and PEGDA-*co*-HEA-SPNS$_{80}$ hydrogels ($\lambda_{excitation}$ = 480 nm). Inset of Fig. (D) shows the picture corresponding to the fluorescence emission of the 3D printed butterfly after UV irradiation with a lamp (λ = 275 nm).

The hydrogels were also capable of emitting fluorescence after visible-light excitation (λ_{exc} = 480 nm) (Fig. 2D). Both hydrogels showed similar fluorescence spectra with a maximum emission peak at 640 nm, which is also characteristic of P3HT SPNs. These results confirm the optical responsivity of the hydrogels in the visible range making them 4D-printable. This effect was proven visually by UV-light excitation of the previously printed butterfly, which exhibited fluorescence as shown in the picture included in the inset of Fig. 2D and Fig. S6 (ESI†).

The photoelectrochemical properties of PEGDA-*co*-HEA-SPNs$_x$ hydrogels were characterized in a three-electrode electrochemical cell using PBS as the electrolyte, a Pt bundle as a counter electrode (CE) and Ag/AgCl as the reference electrode (RE). The hydrogels were sandwiched between a transparent ITO electrode, used as the working electrode (WE), and a glass slide to maintain the hydrogel in electrical contact with the ITO. All the electrodes were immersed in PBS, as schematically reported (Fig. 3A). A photocathodic behavior was recorded when irradiating with a blue LED (λ = 467 nm), with an increase in current for increasing irradiation intensity (Fig. 3B). The photocathodic behavior of P3HT is ascribed to oxygen reduction reactions, as photogenerated electrons from the polymer reduce available species in the electrolyte, *i.e.* oxygen.[31,32] Additionally, the current density increased with increasing concentration of SPNs. Increasing the concentration from 5 to 80, doubled the recorded current, while increasing from 80 to 105 did not show a further increase. Interestingly, the PEGDA-*co*-HEA hydrogels used as a control did not exhibit photocurrent properties.

As previously reported for P3HT thin films and nanoparticles, the metastable photogenerated O_2^- undergoes a fast dismutation in aqueous media resulting in the formation of H_2O_2. Hence, we employed a Black Platinum working electrode to characterize the production of H_2O_2. Black Platinum electrodes have been reported to have a higher sensitivity and selectivity towards H_2O_2.[33–35] The schematic of the electrochemical setup is reported in Fig. 3C, with Pt as CE, Ag/AgCl as RE, and PBS as electrolyte. H_2O_2 generation was recorded only during photostimulation (λ = 467 nm, 67 mW cm^{-2}) (Fig. 3D), whereas when the illumination was switched off, the concentration dropped. An H_2O_2 generation up to ~12 μM, ~13 μM and ~15 μM was recorded for the 5, 80 and 105 mg mL^{-1} nanoparticles concentrations, respectively (Fig. 3E). We chose the lowest irradiation density according to cytotoxicity tests carried out on GL261 cells. The H_2O_2 production did not reflect the concentration dependence demonstrated for the photocathodic recordings. As the photocurrent recording is not selective towards specific chemical species, but rather to the electrons that actually reach the WE, we hypothesize that different reactive species in addition to H_2O_2 were produced.

Prior to photo-stimulation *in vitro* cell tests, the cytotoxicity of the PEGDA-*co*-HEA-SPNs$_x$ hydrogels was tested in contact

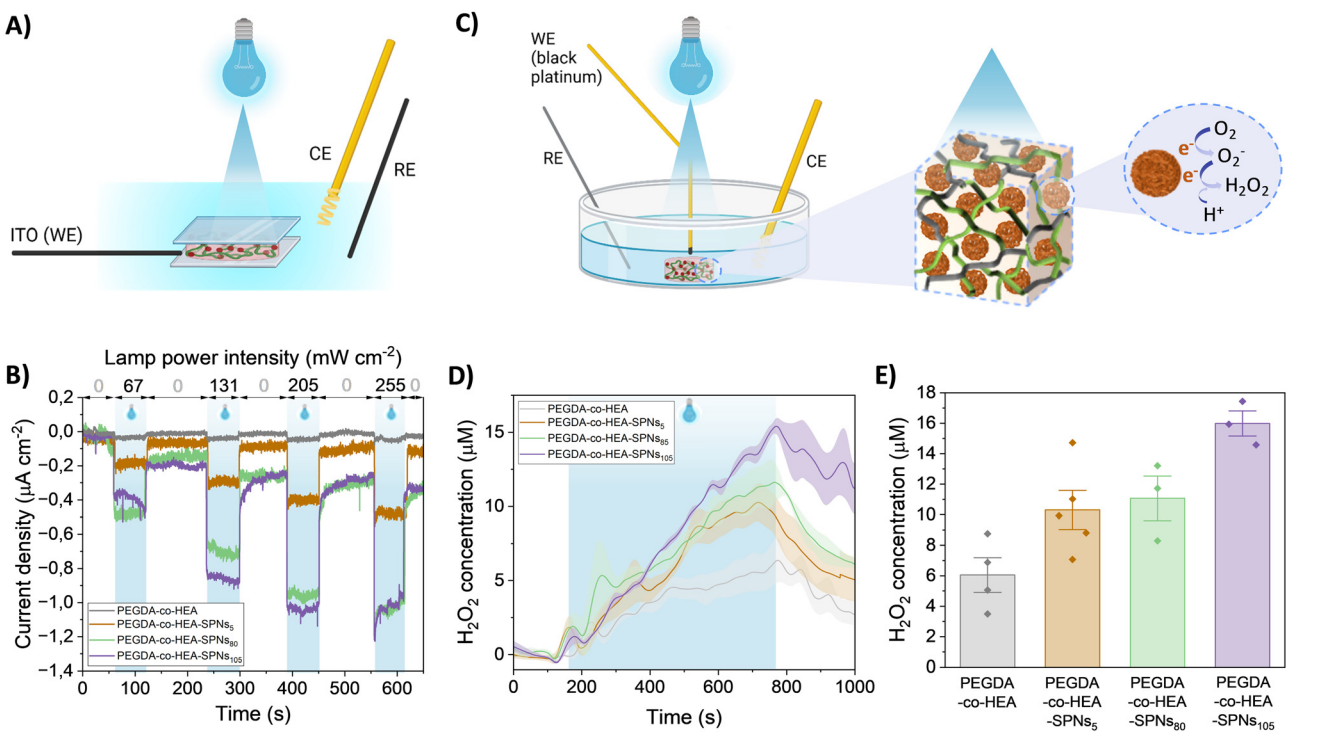

Fig. 3 (A) Schematic representation of the photoelectrochemical cell (PEC) used for measuring the photocurrent properties. (B) Photocurrent density of PEGDA-*co*-HEA-SPNs$_5$ hydrogels upon different ON–OFF irradiation cycles using a LED (λ = 467 nm) at different increasing power intensities (67, 131, 206, and 256 mW cm^{-2}). (C) Schematic representation of the set-up used for measuring the H_2O_2 production, including oxygen reduction reactions following hydrogels irradiation. (D) Spectra of the H_2O_2 produced by the PEGDA-*co*-HEA-SPNs$_x$ hydrogels over time during irradiation (λ = 467 nm, 67 mW cm^{-2}), from 200 s stabilization, and after cutting off the light. (E) Average values (3 replicates) of the H_2O_2 produced by the PEGDA-*co*-HEA-SPNs$_x$ after 10 min irradiation with a LED (λ = 467 nm, 67 mW cm^{-2}).

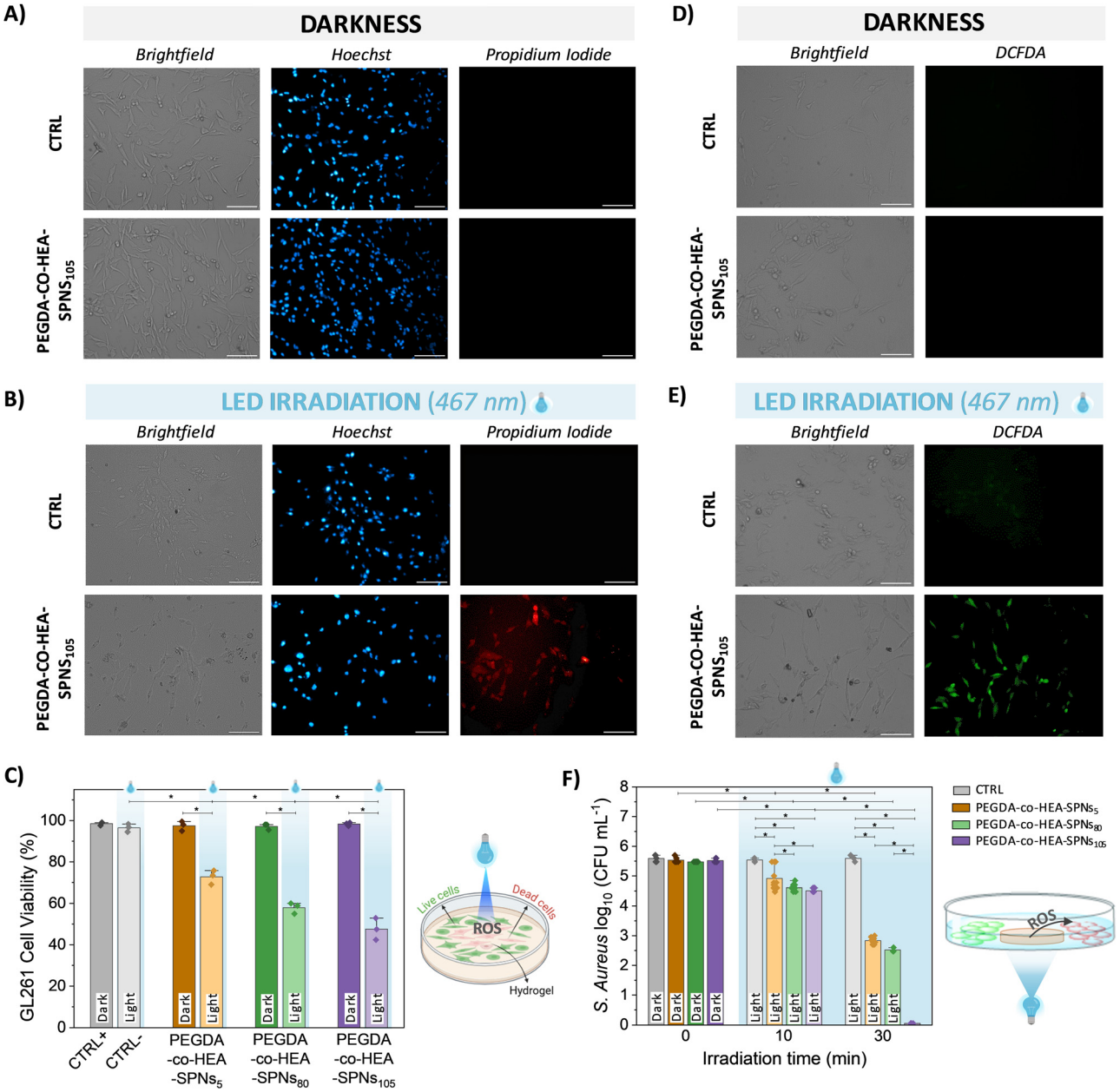

Fig. 4 Fluorescence microscopy images of mouse glioma 261 (GL261) cells in contact with silicone disks used as a control (CTRL) and PEGDA-*co*-HEA-SPNs$_{105}$ hydrogels, (A) before and (B) after LED irradiation (λ = 467 nm; 60 mW cm^{-2}) (40 J cm^{-2}). (C) Flow cytometry results on GL261 cell viability in contact with silicone disks (CTRL) and PEGDA-*co*-HEA-SPNs$_x$ hydrogels, before and after LED irradiation (λ = 467 nm; 60 mW cm^{-2}) for 10 min. The inset includes a schematic representation of the experimental protocol and localized cell death in the irradiated area. Fluorescence images of GL261 cells in contact with silicone disks (CTRL) and PEGDA-*co*-HEA-SPNs$_{105}$ hydrogels, and incubated with the fluorescence probe DCFDA, (D) before and (E) after LED irradiation (λ = 467 nm; 60 mW cm^{-2}) for 10 min. (F) *S. aureus* cells incubated in contact with silicone disks (CTRL) and PEGDA-*co*-HEA-SPNs$_x$ hydrogels, before and after LED irradiation (λ = 467 nm; 60 mW cm^{-2}). The inset includes a schematic representation of the experimental protocol and localized bacteria death in the irradiated area. Dark- and light-coloured bars in diagrams (C) and (F) refer to darkness and illuminated conditions, respectively. Diagrams (C) and (F) include the mean and standard deviation (n = 3) and the ANOVA results at a significance level of *$p < 0.05$ using Tukey's test. Scale bars = 100 μm.

with mouse glioma 261 (GL261) cells (Fig. 4A and C and Fig. S7A, ESI†). GL261 cells were stained with Hoechst (cell nuclei, blue fluorescence) and with propidium iodide (death cell nuclei, red fluorescence). Results indicate that PEGDA-*co*-HEA-SPNs$_x$ hydrogels were not cytotoxic in darkness exhibiting a GL261 cell viability higher than 95% in all cases, without significant differences with respect to the control (CTRL). Then, the hydrogels were irradiated with a LED (λ = 467 nm; 60 mW cm^{-2}, 40 J cm^{-2}) for 10 min (Fig. 4B and Fig. S7B, ESI†). After irradiation, it was observed a decrease in the viability of GL261 cancer cells in contact with the PEGDA-*co*-HEA-SPNs$_x$ hydrogels, whereas those in contact with silicone disks used as

a control remained unaffected. To better quantify the decrease in cell viability, flow cytometry experiments were performed (Fig. 4C and Fig. S8, ESI†). The results indicate that cell viability (CV) decreased with increasing SPNs concentration within the hydrogels, reaching values of 73 ± 3% CV for PEGDA-*co*-HEA-SPNs$_5$, 58 ± 3% CV for PEGDA-*co*-HEA-SPNs$_{80}$ and 48 ± 5% CV for PEGDA-*co*-HEA-SPNs$_{105}$ hydrogels, proving their effectiveness for PDT against GBM. One of the primary mechanisms of PDT involves the production of ROS.[6] Upon photoirradiation with a blue LED light (λ = 467 nm), the PEGDA-*co*-HEA-SPNs$_x$ hydrogels containing photo-active SPNs started to produce ROS, ~12–15 μM H_2O_2 (Fig. 3D and E), that effectively reach GL261 cancer cells in contact with the hydrogels, as proven through fluorescence microscopy by incubating GL261 cells with the 2′,7′-dichlorodihydrofluorescein diacetate (H2-DCF-DA) probe (Fig. 4D, E and Fig. S9, ESI†). Notably, PDT produced cytotoxic ROS only when the hydrogels were activated by light for spatial and temporal controlled PDT against GL261 cancer cells. Furthermore, PDT against Gram-positive *S. aureus* bacteria was also assessed (Fig. 4F). PEGDA-*co*-HEA-SPNs$_x$ hydrogels were not anti-microbial *per se* in the darkness, as no colony forming units (CFU) reduction was observed with respect to the silicone disks used as a control. Nevertheless, upon illumination with a blue LED light (λ = 467 nm, 40 mW cm^{-2}) a decrease in the *S. aureus* CFU viability, induced by ROS production from PEGDA-*co*-HEA-SPNs$_x$ hydrogels, was observed. The *S. aureus* viability decreased with the increasing SPNs concentration in the PEGDA-*co*-HEA-SPNs$_x$ hydrogels, as well as with the irradiation time. A ~ 18% reduction in the *S. aureus* viability was achieved for PEGDA-*co*-HEA-SPNs$_{105}$ hydrogels after 10 min irradiation, and it increased up to ~99% after 30 min irradiation. This photoinduced anti-microbial property plays also a key role in PDT when the photoactive materials and photostimulation probes need to be implanted within the body to avoid infection during and after the implantation. Overall, these results demonstrated the efficacy of the PEGDA-*co*-HEA-SPNs$_x$ hydrogels developed herein for cancer and anti-microbial photodynamic therapies.

3. Materials and methods

3.1. Materials

3-Hexylthiophene ≥98.0% (3HT) was supplied by TCI, iron(III) chloride and methanol ≥99.9% were purchased from Fluka. Tetrahydrofuran (THF), poly(ethylene glycol) diacrylate (PEGDA) >99% and M_n 575, acrylamide (AAm) >99.9%, 2-(hydroxyethyl) acrylate (HEA) >96%, pluronic F-127 (PF-127), Darocur 1173, and phosphate buffer saline (PBS) were purchased from Sigma-Aldrich. Dulbecco's modified Eagle's medium (DMEM), Penicillin 10 000 units mL^{-1}, streptomycin 10 000 μg mL^{-1} solution, glutamine (GlutaMAXTM 100×), trypsin-EDTA Solution 10×, sodium pyruvate 100 mM solution, Hoechst 33342, and Propidium iodide, 2′,7′-dichlorodihydrofluorescein diacetate (DCFH-DA) were purchased from Gibco. Fetal bovine serum (FBS) was purchased from Internegocios S.A. Broth and tryptine-soy agar (TS) were provided by Britania, and D-glucose by Cicarelli. All reagents were used as received.

3.2. Synthesis and characterization of P3HT nanoparticles

Prior nanoparticles synthesis, poly(3-hexylthiophene) (P3HT) was synthesized by oxidative chemical copolymerisation of 3-hexylthiophene, using $FeCl_3$ as an oxidising agent (4 equiv. respect 3HT monomer) and acetonitrile as solvent, at room temperature overnight, as reported previously.[26] The synthesized P3HT possessed a M_n 17 400 g mol^{-1}, as determined by size exclusion chromatography using polystyrene standards, and a regioregularity of 75%, as determined by ^{1}H NMR (Fig. S1, ESI†). Then, P3HT nanoparticles (SPNs) were obtained by flash nanoprecipitation following a previously reported protocol.[28] Briefly, a stock solution of P3HT (1 mg mL^{-1} in THF) containing PF-127 (1 mg mL^{-1} in THF) as surfactant, in a ratio 1 : 9 (%v/v) of P3HT:PF-127, was solubilized at 60 °C for 1 h. Then, 1 mL of this solution was injected into 10 mL of Milli-Q water under stirring at 1300 rpm and 85 °C. Subsequently, the as formed SPNs dispersion was transferred to a beaker to evaporate the THF at 50 °C for 90 min. Finally, the aqueous suspension of SPNs was stored at 4 °C in the darkness for further experiments. The average size of the SPNs was determined by transmission electron microscopy (TEM) using a Talos F200i field emission gun instrument equipped with a Bruker X-Flash100 XEDS spectrometer. SPNs were deposited over carbon-coated copper grids, and dried at room. TEM images were analyzed with the software ImageJ showing an average diameter of 60 ± 6 nm (Fig. S2A, ESI†).

3.3. Synthesis of hydrogels

Hydrogels were synthesized by radical polymerization of acrylic monomers (AAm and HEA) and/or polymers (PEGDA) using P3HT SPNs as the photoinitiator system (PIS) in aqueous media. To that aim, the prepolymer mixture in a ratio 1 : 1 (%v/v) of monomer:SPNs was loaded in a syringe and injected in a glass container (10 mm × 30 mm) of 1 mm thickness sealed with a silicon joint. Then, this vessel was irradiated with a Kessil (PR160L) lamp with a central wavelength of 390 nm (irradiance of 10 mW cm^{-2}), where it absorbs the PIS and not the other components. Three different prepolymer mixtures were prepared, 50%w/w AAm aqueous solution and SPNs in a ratio 1 : 1 (%v/v), PEGDA and SPNs in a ratio 1 : 1 (%v/v), and PEGDA, HEA and SPNs in a ratio 0.5 : 0.5 : 1 (%v/v). The resulting hydrogels were named as PAAm-SPNs$_x$, PEGDA-SPNs$_x$, and PEGDA-*co*-HEA-SPNs$_x$ respectively (where x stands for the SPNs concentration). As a control, hydrogels were prepared by photopolymerization of these acrylic monomers and/or polymer using Darocur 1173 (1%v/v) as a photoinitiator in aqueous media, in a ratio 1 : 1 (%v/v) of monomer:aqueous Darocur, instead of SPNs.

3.4. Photopolymerization kinetics

3.4.1. Fourier transform infrared spectroscopy (FT-IR). To evaluate the performance of P3HT SPNs as photoinitiators, polymerization kinetics were studied by FT-IR using a NICOLET IS20 spectrophotometer (Thermo Scientific) with a resolution

of 1 cm^{-1} and averaging 32 scans. The polymerization conversion was assessed by monitoring the consumption of the vinyl C=C band at 6180 cm^{-1}. The prepolymeric mixtures were loaded into the sealed vessel described above and the spectrum at time 0 was recorded. The mixture was then irradiated with the Kessil lamp (390 nm, 10 mW cm^{-2}). At different time intervals (10, 20, 30, 40, 50, 60, and 80 min), the irradiation was cut off and the FT-IR spectra were recorded. This process was repeated until high conversion (~80% or more) was observed, depending on the pre-polymeric mixture under study.

3.4.2. Photo-rheology. The photopolymerization kinetics and hydrogels formation were studied by photo-rheology through the continuous registration of the elastic modulus (G') and loss modulus (G'') before and after UV irradiation. Photo-rheological measurements were performed with an AR-G2 rheometer (TA Instuments) equipped with a UV-light lamp (365 nm, 5–20 mW cm^{-2}), oscillation stress of 100 Pa, and 0.1 Hz frequency. To prepolymer mixture was placed on a glass parallel plate of 20 mm diameter (300 μm gap) and stabilized for 60 s to be subsequently irradiated for different times, and continuing to register G' and G'' until a plateau was reached.

3.5. Digital light processing (DLP) 3D printing

The prepolymeric mixture was poured into the resin vat of a DLP 3D printer (Anycubic Photon Mono X 6, λ = 405 nm, 2 mW cm^{-2}) and hydrogel structures were printed (layer height = 100 μm, exposure time = 120 s). The printed patterns were first designed with Autodesk Inventor 2021 software.

3.6. Physical–chemical characterization of hydrogels

3.6.1. UV-vis and fluorescence spectroscopies. UV-vis spectra were recorded from 325 to 700 nm with a Shimadzu UV-2550 spectrometer. Fluorescence emission spectra ($\lambda_{excitation}$ = 480 nm) were recorded from 525 to 800 nm with a PerkinElmer LS 55 Fluorescence Spectrometer.

3.6.2. Rheology. The mechanical properties of the hydrogels were determined by oscillatory rheological measurements using an AR-G2 rheometer with a parallel plate configuration of 20 mm diameter and 300 μm gap. Strain sweeps were performed from 0.01 to 1000% strain at 1 Hz. Frequency sweeps were carried out from 0.01 to 10 Hz at 1% strain.

3.6.3. Swelling tests. Prior starting the swelling tests, the hydrogels were weighted (W_0). Then, they were swollen in PBS, at pH 7.4 and room temperature. At established times, the hydrogels were removed from the liquid, externally dried with filter paper to remove excess surface liquid, and weighed (W_t). The swelling percentage (S_w) in wt % was calculated according to eqn 1:

$$S_w = \frac{(W_t - W_0)}{W_0} \times 100 \quad (1)$$

3.7. Electrochemical characterization of photo-responsive hydrogels

The electrochemical characterization of the hydrogels was carried out in a three electrodes electrochemical cell, with PBS as electrolyte, a platinum bundle as counter electrode (CE), Ag/AgCl (Sat) as reference electrode (RE). A VMP3 Biologic potentiostat was employed for electrochemical recording. The cell was kept in a Faraday cage to reduce electrical noise. For all the electrochemical measurement, the hydrogels were soaked in PBS overnight at 4 °C in the dark, and the measurements were carried out the day after soaking.

3.7.1. Photocurrent. Square PEGDA-SPNs$_x$ hydrogels (x = 5, 80 and 105 mg mL^{-1}) of 10 mm × 10 mm and 1 mm thickness were placed between a glass and an ITO electrode. A Kessil (PR160L) lamp with 467 nm central wavelength was employed for the photostimulation, with four intensity steps corresponding to 67, 131, 206 and 256 mW cm^{-2}. The illumination was carried out from the glass side. The photocurrent was recorded at open circuit voltage.

3.7.2. H_2O_2 production. For the H_2O_2 recording, black platinum electrodes were prepared according to reported procedures,[34–36] to increase the sensitivity towards hydrogen peroxide. Briefly, black platinum was electrodeposited on Platinum wires (300 μm diameter) in a three electrodes electrochemical cell, with a Pt bundle as CE and a Ag/AgCl saturated KCl as RE, in a 31.2 mM solution of hexachloroplatinic acid in PBS as electrolyte. The electrodes were all characterized first by cyclic voltammetry in a freshly prepared 10 mM solution of H_2O_2 in PBS, identifying reduction and oxidation peaks. Then, the electrodes were washed and calibrated in a fresh PBS solution keeping the WE at the H_2O_2 oxidation potential. After calibration, the H_2O_2 production from the PEGDA-SPNs$_x$ (x = 5, 80 and 105 mg mL^{-1}) hydrogels was evaluated. A 10 mm × 10 mm piece of hydrogel (previously soaked overnight in PBS) was placed at the bottom of a Petri dish. The CE (Pt bundle) and RE (Ag/AgCl saturated KCl) were placed on the sides, the electrolyte was fresh PBS. The black platinum working electrode was placed on top of the hydrogel with a micromanipulator. The illumination was carried out with the same Kessil lamp (467 nm central wavelength) used for the photocurrent characterization. We employed a single intensity, namely 67 mW cm^{-2}, as indicated by cell viability experiments. The electrode was kept at the oxidation potential, and the current was converted to the concentration through the calibration curve previously mentioned. In between each experiment, the electrodes were thoroughly washed and fresh PBS was added for each condition.

3.8. *In vitro* cell culture tests

Prior to cell seeding, PEGDA-*co*-HEA-SPNs$_x$ (x = 5, 80 and 105 mg mL^{-1}) hydrogels were formed by photopolymerization (390 nm, 10 mW cm^{-2}) in silicon molds of 10 mm diameter and 1 mm thickness for 6000 s. Then, PEGDA-SPNs$_x$ (x = 5, 80 and 105 mg mL^{-1}) hydrogels were placed in a 24-well plate and washed with 1 mL of PBS under sterile conditions for 3 days to remove non-reacted monomers by replacing the washing PBS solution daily.

3.8.1. Cell viability assay. GL261 cells were subcultured post-thawing for two passages, achieving 70 to 80% confluence. Following trypsinization, cells were counted and seeded at a density of 2 × 10^5 cells mL^{-1} (500 μL per well) in 24-well plates,

subsequently undergoing a 24-hour incubation period. Hydrogels were simultaneously soaked with complete cell culture media on a 24-well plate for 24 hours at 37 °C prior to cell assays. Following the incubation period, the medium was replaced with fresh media enriched with 10% FBS, accompanied by a small silicone piece (used as a control) or different PEGDA-*co*-HEA-SPNs$_x$ hydrogels. The treatments were divided between those that were not exposed to irradiation (darkness) and those that were irradiated to evaluate the phototherapeutic effect. Afterwards, cells in contact with hydrogels were irradiated with a custom-designed multi light emitting diodes (LED) system equipped with LED arrays (maximum wavelength of 467 ± 20 nm) with an irradiance of 60 mW cm^{-2} for 10 min (40 J cm^{-2}). After the irradiation procedure, hydrogels were carefully removed, and the culture medium was replaced to evaluate cell viability 24 h post-treatment by observing morphological changes (using brightfield and fluorescence microscopy, in a Nikon Eclipse Ti–S microscope equipped with a LWD 20×/0.4 objective lens and a Nikon DS-QiMC CCD camera). Cell nuclei staining was performed with Hoechst 33342 1 μg mL^{-1} for 10 min and cell dead staining was performed with Propidium iodide (0.015 μM). Two sets of independent experiments were performed (with n = 3 for hydrogel sample). Cell death was quantified following cell detachment with a trypsin solution. The analysis was conducted using a Guava EasyCyte 6 2L flow cytometer, and the data were processed with FlowJo software (version 10).

3.8.2. ROS production evaluation. Intracellular ROS after PDT treatment was detected using DCFH-DA fluorescent probe. GBM cells were cultured in 24-well plate (1 × 10^5 cell per well) and treated as follows. Cells were exposed to different hydrogels and irradiated as previously described. Immediately after treatment, cells were incubated with 10 μM DCFH-DA at 37 °C for 30 min. The 2′,7′-dichlorofluorescin (DCF) fluorescence was recorded by fluorescence microscopy. Growing cells without any treatment and exposed to silicone discs were used as negative control.

3.9. Antimicrobial tests

3.9.1. Strain maintenance. A strain of MRSA 773 bacteria obtained from a previous clinical isolation was used.[37] The bacterial culture was stored in TS broth with 10% glycerol at −40 °C. The bacterial inoculum was grown under aerobic conditions on TS agar in an oven at 35 °C and in TS broth in an oven with shaking (100 rpm) at 35 °C for 18 h.

3.9.2. Microbial photodynamic therapy. A colony isolated from a pure culture was taken and incubated in 5 mL of TS broth for 18 h. Then, 20 μL of this suspension was taken and placed in 2 mL of TS broth solution and grown under agitation (100 rpm) at 37 °C until an optical density of 0.2 at 600 nm (OD600) was reached; this is done to obtain a metabolically active population (logarithmic phase of microbial growth).[38] Once the desired OD was reached, a 1/1000 dilution in 10% glucose (inoculum) was prepared and the concentration of this inoculum was 106 CFU mL^{-1}. In parallel, hydrogel discs of ∼7 mm were cut, washed three times for 10 minutes each using distilled water, and then the procedure was repeated using ethanol (both solvents previously sterilized with ultraviolet light). Subsequently, a 500 μL aliquot of the cell suspensions was placed in sterile 48-well polystyrene plates. A silicone disc (CTRL) or PEGDA-*co*-HEA-SPNs$_x$ hydrogels were added to each well. The plate was incubated in the dark for 60 min at 35 °C and then the plate was irradiated with a LED light (λ = 395 nm; 29.4 ± 0.3 mW cm^{-2}) on the sample plane for different times (10 and 30 min). After irradiation, 20 μL was taken from each well and 4 serial 1/10 dilutions were made in PBS buffer (in order to dilute the bacterial load sufficiently to be able to count). 10 μL of each dilution was seeded on a TS agar plate, serial dilutions were performed and 10 μL of each dilution was seeded on a TS agar plate. They were incubated for 18–24 h and colony counts were carried out (then multiply by the dilution factor performed to obtain the number of CFU mL^{-1}). All assays were performed in triplicate and the results were represented as mean ± standard deviation.

3.10. Statistical analysis

Statistical analyses were performed using one-way ANOVA, at a significance level of $^*p < 0.05$, using Tukey's multiple comparison test.

4. Conclusions

In this work, P3HT SPNs were successfully employed both as photoinitiators of acrylic hydrogels and as photosensitizers for PDT. First, P3HT SPNs induced the visible light-photopolymerization of acrylic monomers (AAm, HEA, and PEGDA) leading to the formation of PAAm-SPNs, PEGDA-SPNs, and PEGDA-*co*-HEA-SPNs hydrogels. They also acted as active photosensitizers when embedded within the hydrogels to trigger the production of H_2O_2, a kind of ROS used for photodynamic therapies. The effect of SPNs concentration on the photopolymerization kinetics, photocurrent properties, and ROS production of the hydrogels was studied, and results pointed out an enhanced localized PDT performance with increasing SPNs concentration as expected. PEGDA-*co*-HEA-SPNs$_{105}$ hydrogels decreased a ∼50% GL261 cancer cells viability upon irradiation with a visible blue LED light. Moreover, PEGDA-*co*-HEA-SPNs$_{105}$ hydrogels also presented antimicrobial properties with ∼99% reduction *S. aureus* viability after 30 min irradiation with a visible blue LED light. All in all, these results show that the intelligent P3HT acrylic hydrogels developed in this work are promising materials for PDT against both cancer cells and bacteria.

Author contributions

R. N. A. experimental research, formal analysis, and writing. I. A. A. photocurrent and ROS production experiments, formal analysis, and writing. M. C. *in vitro* cell tests and formal analysis. A. S. L. *in vitro* antimicrobial tests and formal analysis. L. E. I. *in vitro* cell tests, formal analysis, and writing. A. G. experimental research. C. A. C. supervision. L. M. G.

supervision. D. M. funding acquisition, writing, and reviewing. R. E. P. supervision, writing, and reviewing. M. C-G. conceptualization, rheological experiments, formal analysis, supervision, funding acquisition, writing, review, and editing.

Data availability

The data supporting this article have been included as part of the ESI.†

Conflicts of interest

There are no conflicts to declare.

Acknowledgements

The authors acknowledge the grant PID2020–119026GB-I00 funded by MCIN/AEI/10.13039/501100011033. M. C.-G. thanks ''Ayuda RYC2022-036380-I financiada por MICIU/AEI/10.13039/501100011033 y por el FSE +'' and the Emakiker program of POLYMAT (UPV/EHU). This work was funded by the European Union under GA no. 101129945 ''IONBIKE 2.0'', and the European Union's Horizon 2020 research and innovation programme under the Marie Sklodowska-Curie grant agreement No. 101034379. Authors also appreciate financial support from SECyT UNRC (PPI 2024), ANPCyT (PICT 2020/3803) and CONICET (PIP 11220200102377CO01). R. N. A., M. C., A. S. L. thanks CONICET for his doctoral scholarships. C. A. C., M. L. G., and R. E. P. are permanent research staff of CONICET.

References

1 A. N. Kolodkin, R. P. Sharma, A. M. Colangelo, A. Ignatenko, F. Martorana, D. Jennen, J. J. Briedé, N. Brady, M. Barberis, T. D. G. A. Mondeel, M. Papa, V. Kumar, B. Peters, A. Skupin, L. Alberghina, R. Balling and H. V. Westerhoff, *NPJ Syst. Biol. Appl.*, 2020, **6**, 34.
2 M. Criado-Gonzalez and D. Mecerreyes, *J. Mater. Chem. B*, 2022, **10**, 7206–7221.
3 B. A. Cesca, M. D. Caverzan, M. J. Lamberti and L. E. Ibarra, *Int. J. Mol. Sci.*, 2024, **25**, 7525.
4 A. Rahman, S. Pallichankandy, F. Thayyullathil and S. Galadari, *Free Radicals Biol. Med.*, 2019, **134**, 527–544.
5 B. Perillo, M. Di Donato, A. Pezone, E. Di Zazzo, P. Giovannelli, G. Galasso, G. Castoria and A. Migliaccio, *Exp. Mol. Med.*, 2020, **52**, 192–203.
6 G. Li, C. Wang, B. Jin, T. Sun, K. Sun, S. Wang and Z. Fan, *Cell Death Discovery*, 2024, **10**, 466.
7 M. Miretti, M. A. González Graglia, A. I. Suárez and C. G. Prucca, *J. Photochem. Photobiol.*, 2023, **13**, 100161.
8 L. E. Ibarra, M. L. Vilchez, M. D. Caverzán and L. N. Milla Sanabria, *J. Neurosci. Res.*, 2021, **99**, 1024–1047.
9 H. Yang, R. Liu, Y. Xu, L. Qian and Z. Dai, *Nano-Micro Lett.*, 2021, **13**, 35.
10 X. Wang, T. Li, H. Ma, D. Zhai, C. Jiang, J. Chang, J. Wang and C. Wu, *NPG Asia Mater.*, 2017, **9**, e376–e376.
11 R. C. Advincula, J. R. C. Dizon, E. B. Caldona, R. A. Viers, F. D. C. Siacor, R. D. Maalihan and A. H. Espera, *MRS Commun.*, 2021, **11**, 539–553.
12 J. Chakraborty, J. Fernández-Pérez, M. Takhsha Ghahfarokhi, K. A. van Kampen, T. ten Brink, J. Ramis, M. Kalogeropoulou, R. Cabassi, C. de Julián Fernández, F. Albertini, C. Mota, S. Ghosh and L. Moroni, *Cell Rep. Phys. Sci.*, 2024, **5**, 101819.
13 A. Hernández-Sosa, R. A. Ramírez-Jiménez, L. Rojo, F. Boulmedais, M. R. Aguilar, M. Criado-Gonzalez and R. Hernández, *Polymers*, 2022, **14**, 2229.
14 M. Caprioli, I. Roppolo, A. Chiappone, L. Larush, C. F. Pirri and S. Magdassi, *Nat. Commun.*, 2021, **12**, 2462.
15 M. Criado-Gonzalez, A. Dominguez-Alfaro, N. Lopez-Larrea, N. Alegret and D. Mecerreyes, *ACS Appl. Polym. Mater.*, 2021, **3**, 2865–2883.
16 H. B. D. Tran, C. Vazquez-Martel, S. O. Catt, Y. Jia, M. Tsotsalas, C. A. Spiegel and E. Blasco, *Adv. Funct. Mater.*, 2024, **34**, 2315238.
17 C. A. Spiegel, M. Hackner, V. P. Bothe, J. P. Spatz and E. Blasco, *Adv. Funct. Mater.*, 2022, **32**, 2110580.
18 N. Ballard and J. M. Asua, *Prog. Polym. Sci.*, 2018, **79**, 40–60.
19 M. Regato-Herbella, D. Mantione, A. Blachman, A. Gallastegui, G. C. Calabrese, S. E. Moya, D. Mecerreyes and M. Criado-Gonzalez, *ACS Macro Lett.*, 2024, **13**, 1119–1126.
20 F. Dumur, *Eur. Polym. J.*, 2022, **169**, 111120.
21 E. R. Zhiganshina, M. V. Arsenyev, D. A. Chubich, D. A. Kolymagin, A. V. Pisarenko, D. S. Burkatovsky, E. V. Baranov, A. G. Vitukhnovsky, A. N. Lobanov, R. P. Matital, D. Y. Aleynik and S. A. Chesnokov, *Eur. Polym. J.*, 2022, **162**, 110917.
22 A. Gallastegui, R. M. Spada, G. Cagnetta, R. A. Ponzio, S. R. Martínez, C. M. Previtali, M. L. Gómez, R. E. Palacios and C. A. Chesta, *Macromol. Rapid Commun.*, 2020, **41**, 2070019.
23 G. E. Cagnetta, A. Gallastegui, S. R. Martínez, D. Mantione, M. Criado-Gonzalez, M. Regato-Herbella, L. Lezama, R. E. Palacios, M. L. Gómez, D. Mecerreyes and C. A. Chesta, *Macromolecules*, 2024, **57**, 78–87.
24 G. E. Cagnetta, S. R. Martínez, L. E. Ibarra, A. Gallastegui, J. F. Martucci, R. E. Palacios, C. A. Chesta and M. L. Gómez, *Biomater. Adv.*, 2023, **149**, 213399.
25 F. Lodola, V. Rosti, G. Tullii, A. Desii, L. Tapella, P. Catarsi, D. Lim, F. Moccia and M. R. Antognazza, *Sci. Adv.*, 2019, **5**, eaav4620.
26 M. Criado-Gonzalez, L. Bondi, C. Marzuoli, E. Gutierrez-Fernandez, G. Tullii, C. Ronchi, E. Gabirondo, H. Sardon, S. Rapino, M. Malferrari, T. Cramer, M. R. Antognazza and D. Mecerreyes, *ACS Appl. Mater. Interfaces*, 2023, **15**, 35973–35985.
27 G. Tullii, E. Gutierrez-Fernandez, C. Ronchi, C. Bellacanzone, L. Bondi, M. Criado-Gonzalez, P. Lagonegro, F. Moccia, T. Cramer, D. Mecerreyes, J. Martín and M. R. Antognazza, *Nanoscale*, 2023, **15**, 18716–18726.
28 M. Criado-Gonzalez, C. Marzuoli, L. Bondi, E. Gutierrez-Fernandez, G. Tullii, P. Lagonegro, O. Sanz, T. Cramer, M. R. Antognazza and D. Mecerreyes, *Nano Lett.*, 2024, **24**, 7244–7251.

29 M. Regato-Herbella, I. Morhenn, D. Mantione, G. Pascuzzi, A. Gallastegui, A. B. Caribé dos Santos Valle, S. E. Moya, M. Criado-Gonzalez and D. Mecerreyes, *Chem. Mater.*, 2024, **36**, 1262–1272.
30 E. Yarali, M. J. Mirzaali, A. Ghalayaniesfahani, A. Accardo, P. J. Diaz-Payno and A. A. Zadpoor, *Adv. Mater.*, 2024, **36**, 2402301.
31 I. Abdel Aziz, M. Malferrari, F. Roggiani, G. Tullii, S. Rapino and M. R. Antognazza, *iScience*, 2020, **23**, 101091.
32 L. Bondi, C. Marzuoli, E. Gutiérrez-Fernández, G. Tullii, J. Martín, B. Fraboni, D. Mecerreyes, M. R. Antognazza and T. Cramer, *Adv. Electron. Mater.*, 2023, **9**, 2300146.
33 B. Ilic, D. Czaplewski, P. Neuzil, T. Stanczyk, J. Blough and G. J. Maclay, *J. Mater. Sci.*, 2000, **35**, 3447–3457.
34 S. Ben-Amor, E. Vanhove, F. Sékli Belaïdi, S. Charlot, D. Colin, M. Rigoulet, A. Devin, N. Sojic, J. Launay, P. Temple-Boyer and S. Arbault, *Electrochim. Acta*, 2014, **126**, 171–178.
35 S. E. Stanca, F. Hänschke, A. Ihring, G. Zieger, J. Dellith, E. Kessler and H. G. Meyer, *Sci. Rep.*, 2017, **7**, 1074.
36 S.-E. Stanca, O. Vogt, G. Zieger, A. Ihring, J. Dellith, A. Undisz, M. Rettenmayr and H. Schmidt, *Commun. Chem.*, 2021, **4**, 98.
37 A. Ahmad, A. Khan, N. Manzoor and L. A. Khan, *Microb. Pathog.*, 2010, **48**, 35–41.
38 S. R. Martínez, L. E. Ibarra, R. A. Ponzio, M. V. Forcone, A. B. Wendel, C. A. Chesta, M. B. Spesia and R. E. Palacios, *ACS Infect. Dis.*, 2020, **6**, 2202–2213.

